IN-SITU DEFECT DETECTION FOR LASER POWDER BED FUSION WITH ACTIVE LASER THERMOGRAPHY

P. P. Breese*, T. Becker*, S. Oster*, C. Metz†, and S. J. Altenburg*

*Bundesanstalt für Materialforschung und -prüfung (BAM), Berlin, Germany 12489
†THETASCAN GmbH, Dinslaken, Germany 46535

Abstract

Defects are still common in metal components built with Additive Manufacturing (AM). Process monitoring methods for laser powder bed fusion (PBF-LB/M) are used in industry, but relationships between monitoring data and defect formation are not fully understood yet. Additionally, defects and deformations may develop with a time delay to the laser energy input. Thus, currently, the component quality is only determinable after the finished process.

Here, active laser thermography, a nondestructive testing method, is adapted to PBF-LB/M, using the defocused process laser as heat source. The testing can be performed layer by layer throughout the manufacturing process. We study our proposed testing method along experiments carried out on a custom research PBF-LB/M machine using infrared (IR) cameras.

Our work enables a shift from post-process testing of components towards in-situ testing during the AM process. The actual component quality is evaluated in the process chamber and defects can be detected between layers.

Introduction and Motivation

Additive Manufacturing (AM) of metals as a novel and complex technique is still prone to defects and unwanted process deviations causing them. Defects in the finished components may include cracks [1], porosity [2], and geometric deviations, among others. These defects can lead to reduced component properties and quality [3], so that time-consuming reworks and even rejects become unavoidable. Therefore, a suited quality control for AM is necessary. This is currently done in two ways: on the one hand, via in-situ monitoring of the AM process itself, e.g., of the melt pool over time. This is admittedly helpful as process quality and component quality are indeed directly related, but not sufficient as the actual component status during manufacturing is not fully determinable. On the other hand, currently, a subsequent ex-situ testing is necessary to determine the actual component status, e.g., via X-ray computer tomography. For safety critical components this testing is needed, but is also very time-consuming, and rejects are detected only after the finished AM process.

Due to this, a high optimization potential lies within shifting from ex-situ testing towards nondestructive in-situ testing (NDT). The actual quality and status of the built AM component would become determinable during the process. For this, we introduce the possibility of using active laser thermography (or active laser thermographic testing, TT) as an NDT procedure in each layer of the build process. This novel approach is applied on laser powder bed fusion of metals (PBF-LB/M) with 316L stainless steel in the following. For comparison purposes, the common in-situ monitoring technique of optical tomography (OT) is also used simultaneously in each layer. In the following, after further general insights and the experimental methods, the results of OT as monitoring and TT as testing are compared and discussed. Thereby, an initial assessment of the in-situ TT for AM approach is possible, and gathered insights may be used for future works.

Background

In the following, the two used techniques for AM process and component assessment are introduced: optical tomography as process monitoring method on the one hand, and active laser thermographic testing as nondestructive testing method on the other hand.

Optical Tomography (OT)

OT is a current AM process monitoring technique used for PBF-LB/M. [4] Classically, a single camera in the visual or near-infrared wavelength range is monitoring the powder bed. It is used for long-time exposures throughout a complete manufactured layer. In this way, the emitted radiation of the AM process in the observed wavelength range is captured. Due to the integration over time, no temporal information is available, but highly spatially resolved data for the whole layer. From this, conclusions about the local process quality can be drawn. It currently finds rise in popularity due to low hardware costs as well as a simple general usage.

Active Laser Thermographic Testing (TT)

For the NDT technique of active laser thermography, heat is introduced via a laser onto the surface of the tested object. The resulting thermal response of the unsteady heat flux is captured via an IR camera. Using additional algorithms for analysis, defects are detectable in this way due to several occurring effects. These effects include altered local thermal properties or altered local laser absorptivity, among others. The approach of scanning over the test object's surface with a laser spot is often referred to as flying spot thermography. With it, surface defects like open cracks are detectable. [5] This approach was for example also applied on the PBF-LB/M process by Herzer and Schilp utilizing the process laser. [6] However, the introduced energy per area was rather high (no NDT approach), and solely information of a single testing scan track and not the scanning sequence as a whole was taken into account. In a prior work, we could show on a test specimen that nondestructive testing inside a PBF-LB/M machine is possible via defocusing the process laser. [7] Based on this, we incorporate this approach into the actual AM process, and take another step towards a nondestructive in-situ testing for PBF-LB/M.

Experimental Setup and Methods

This section describes the setup and methods used in this study: the PBF-LB/M research machine, the camera setups (OT and TT), the AM build job along with the incorporated artificial defects, and the thermographic testing routine. Furthermore, the analysis of the recorded data is described.

PBF-LB/M Research Machine - SAMMIE

To optimize controllability and data accessibility, a noncommercial PBF-LB/M research machine was successfully developed at the BAM facilities in Berlin-Adlershof. The Sensor-based Additive Manufacturing Machine (SAMMIE) was set up in this study as illustrated in Figure 1. It portrays the elements of SAMMIE, beginning with the laser path including focus unit (varioSCAN by SCANLAB) and a galvanometer scanner (intelliSCAN by SCANLAB). The laser source employed is an ytterbium continuous wave fiber laser (IPG Photonics) operating at 1070 nm,

capable of generating a maximum nominal power of 500 W. Control over the manufacturing process and the laser path components is achieved through the Direct Machining Control (DMC) software. A shielding gas system with filter ensures a process at low oxygen levels. Finally, the configuration includes a process chamber with a powder bed unit inside with a build volume of 50 x 70 x 35 mm³. An outstanding feature of SAMMIE is its capacity to host multiple camera systems simultaneously during the active process. The off-axis arrangement of the cameras at the process chamber's optical entry points allows observing the entire powder bed from a close proximity. Furthermore, it is feasible to implement on-axis camera installations along the laser path, enabling precise monitoring of the laser affected zone. However, although not utilized in this publication, the on-axis capability is intended for future investigations. The entire PBF-LB/M process operation is controlled by LabVIEW-based software (National Instruments) which ensures a fully accessible AM process with SAMMIE. Moreover, additional procedures may be incorporated such as active laser thermographic testing after a finished layer.
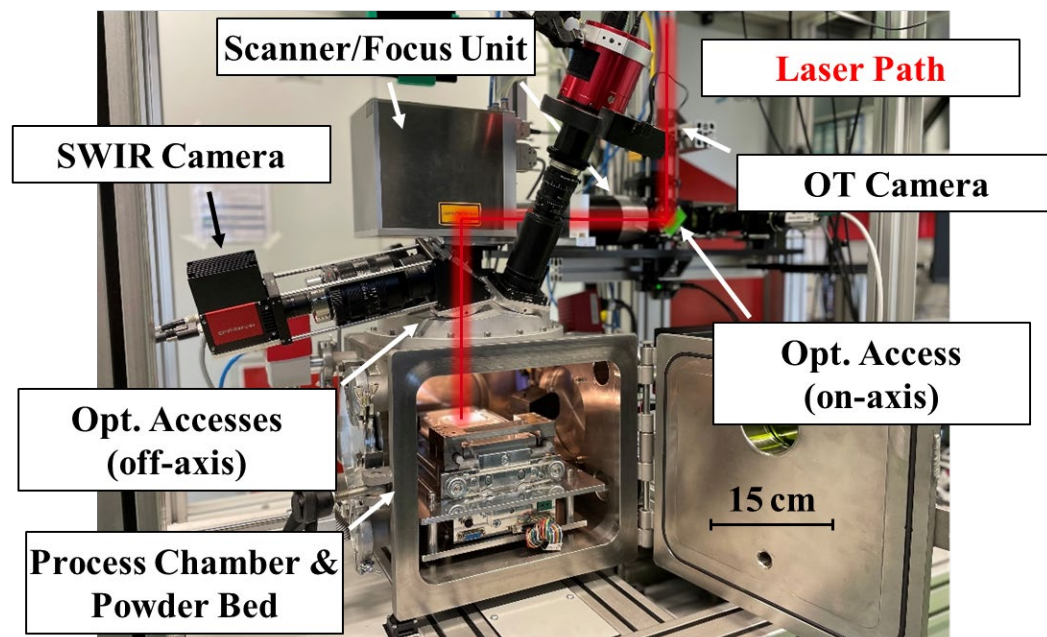

Figure 1: Overview of the utilized PBF-LB/M research machine SAMMIE.

Camera Setups

For the comparison of monitoring and testing, an optical tomography and a thermographic testing setup were installed at SAMMIE. The OT setup comprised of a ZWO ASI 6200 MM Pro Mono camera with a full-frame resolution of 62 Mpx (9576 x 6388 px²) at 16-bit image depth. The camera was mounted on top of the process chamber using a 100 mm objective (cf. Figure 1). This resulted in a spatial resolution of approximately 10 µm/px when focusing on the build platform. Filters were installed in the optical path to ensure optimal conditions for the recorded images. Firstly, a bandpass filter at 725 nm was included. Secondly, neutral density (ND) filters at varying strengths were incorporated via a filter wheel to switch between them effortlessly. The ND filter suited best was a ND2.2 (0.63% transmittance) at 725 nm. With this setup, monochromatic OT longtime exposures at full dynamic range were possible.

For the thermographic testing data acquisition, the Goldeye CL-033 TEC1 camera by Allied Vision operating in the short-wave infrared (SWIR) range was used (cf. also Figure 1). Its built-in InGaAs sensor gives a spectral sensitivity spanning from 0.9 µm to 1.7 µm. The camera captures images at a full-frame resolution of 640 x 512 px² with a 14-bit image depth and a frame rate of 234 Hz. For focusing on the build plane, the camera was equipped with a 100 mm SWIR lens. An extension tube, approximately 35 mm in length, was included to achieve the desired focus. Consequently, a spatial resolution of 40 µm/px was achieved. Moreover, a notch filter (NF1064-44 by Thorlabs) at the laser wavelength was positioned in front of the camera objective. This ensured that only the thermal response was captured while excluding the reflected laser itself. The camera system was installed off-axis at one of the optical access points of the SAMMIE process chamber using an adjustable mirror system. This configuration facilitated alignment between the recorded camera images and the region of interest on the build plane.

Build Job and Defects

The PBF-LB/M build process was performed on the research machine SAMMIE with 316L stainless steel powder (1.4404) as base material. Particle sizes ranged from 10 µm up to 45 µm (d_{50} = 32.55 µm). The process itself was conducted under argon shielding gas atmosphere at a laser power of 167 W and a scanning speed of 700 mm/s (monodirectional) while the layer height was set to 40 µm. The hatching distance between scan tracks was at 100 µm while the laser spot diameter (D_{86}) was at approximately 80 µm.

Throughout the manufacturing process of the monitored and tested component, two separate zones with artificial defects were implemented. These defects were omitted areas where no scanning and therefore no powder melting took place. The first zone comprised 24 round defects (cf. Figure 2a) with 12 cylindrical (top of the figure) and 12 spherical shapes (bottom of the figure) which ranged from layers 75 to 87. In this zone, laser scanning directions changed by 67 degrees between each layer. Defect diameters were at 1.5 mm down to 400 µm in steps of 100 µm. The second zone included defective areas in the form of narrow triangles and notches (cf. Figure 2b). This artificially recreates (powder filled) crack structures in the AM component. They were included in the layers 140 to 149 and are open to the top. The laser scanning directions were kept constant between layers and parallel to the crack structures to ensure precise manufacturing. To even enhance the right edge of the left triangle, the edge was scanned separately with 3 degrees scanning angle. The two triangles had a maximum width of 1.1 mm. The notch widths ranged from 400 µm to 100 µm in steps of 100 µm while their length was at 8 mm. With these two defect zones, different types of defects were analyzable.
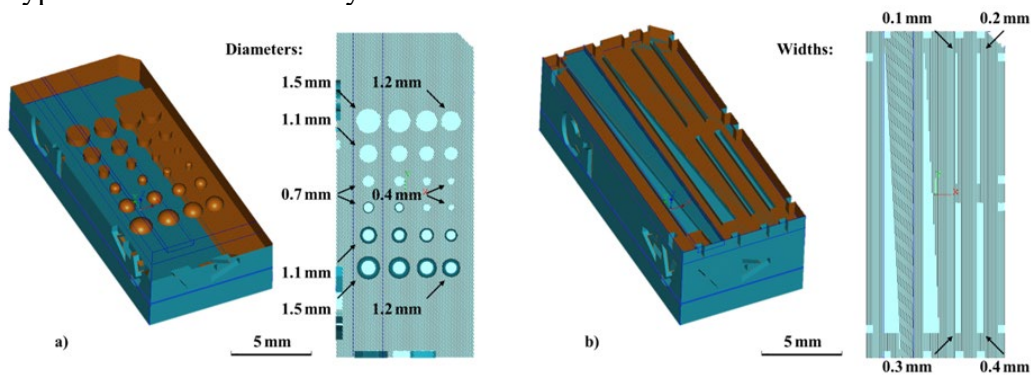

Figure 2: Internal artificial defects in the manufactured component with cylindrical and spherical defects in the first zone (a) and notch defects in the second zone (b).

Thermographic Testing and Analysis

While the OT solely required a longtime exposure during manufacturing of a layer, the active laser thermography required an additional energy input via the defocused process laser. This scanning over the component's surface was executed after every layer in an area of 8.5 x 16.5 mm² right across the defective regions. Appropriate scanning parameters had to be found empirically to ensure an energy input as low as possible for the sake of non-destructiveness of testing. However, energy input had to be high enough that the SWIR camera was able to capture the thermal response. The utilized thermographic testing parameters were at 32 W laser power with a scanning speed of 22 mm/s (monodirectional). The distance between scan tracks was 250 µm which resulted in 67 lines for the tested area. The defocused process laser had a spot diameter (D_{86}) of approximately 1.1 mm. The off-axis SWIR camera was recording with a framerate of 235 Hz at an exposure time of $t_{exp} = 200$ µs with an aperture of 22.

For the analysis of the thermographic data, the maximum thermograms were investigated. For every pixel, the maximum thermal response in the whole recorded testing sequence was found and displayed to create the maximum thermogram. This was done for every layer. Background is that the information content of a single frame is rather low, so the sequence as a whole is taken into account. The highest recorded thermal response for a specific pixel (which corresponds to a specific location on the AM component surface) gives information on the regional thermal properties. With this, surface defects can be localized as they alter the thermal properties of the AM component locally. Additionally, to assess the potential of detecting subsurface defects by active laser thermography, the sum thermogram was investigated. In this case, the sum of the recorded thermal signal was calculated for every pixel. This also takes the cooling behavior into account. It was investigated for layer 89, so two layers after the round defects were closed by sound, complete layers. Therefore, the nominal defect depth was at 80 µm. To enhance contrast in the sum thermogram, the exposure time of the SWIR camera was increased to $t_{exp} = 500$ µs for this layer.

As both, optical tomography and thermographic testing, were conducted off-axis from different positions, perspective transformations were performed. [8] In this way, optical distortions were removed and comparability between monitoring and testing was enhanced.

Results and Discussion

In the following, the obtained images of the optical tomography as monitoring method and the thermographic testing as nondestructive testing approach are compared. This is done layer by layer for the first zone with round defects (layers 86 to 89) and for the second zone with notch defects (layer 144). Goal is to determine the current capabilities of the in-situ TT as a novel approach for PBF-LB/M in comparison to the OT as in-situ monitoring.

Round Defects

Figure 3 shows the obtained images for layer 86 of the long-time exposure OT on the left (a) and the maximum thermogram of the TT on the right (b). The perspective transformation corrected perspective distortions introduced by the off-axis configurations for both methods. This allows an improved comparison. In the OT image, missing process scan tracks are apparent. This was due to the capture delay of the used high-resolution OT camera, thus scans at the beginning of the layer manufacturing are missing. However, the comparison of OT and TT was still feasible, and

therefore, the data recording was deemed successful. The OT clearly shows the omitted areas of the artificial round defects. All diameters down to 400 µm were resolved with ease due to the high spatial resolution of the utilized camera.
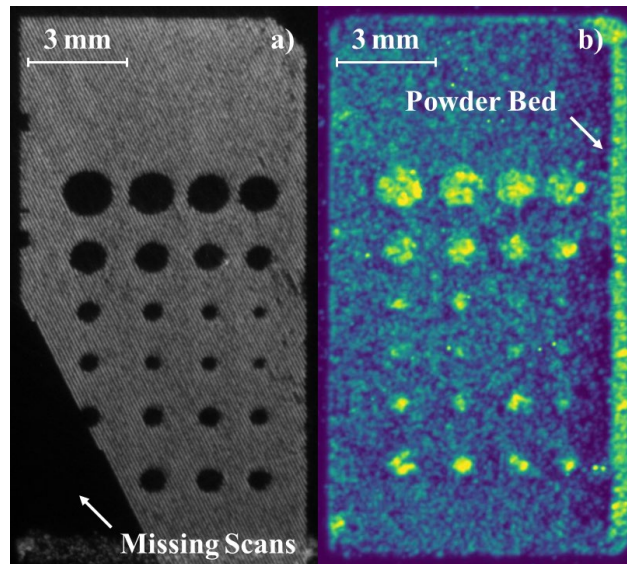

Figure 3: Optical Tomography (a) and Thermographic Testing (b) results of layer 86. Cylindrical and spherical artificial defects are at full diameters.

The incorporation of an in-situ thermographic testing routine into the PBF-LB/M process was successful as Figure 3b shows. This marks a great step on the way to include in-situ NDT into AM because to our knowledge, a nondestructive TT implementation without remelting was not achieved before. The selection of the SWIR spectral range for the IR camera was motivated by the planned on-axis experiments including active laser thermography. The laser path, specifically the focus unit, is optimized for transmissivity at a laser wavelength of 1070 nm which makes the neighboring SWIR range most suitable for a transfer to on-axis operation. However, in the current investigation, off-axis experiments were conducted to explore the general feasibility of the approach. Furthermore, the same SWIR camera setup would allow for additional in-process monitoring of the melt pool. Additionally, SWIR cameras are comparatively more affordable than cooled mid-wave infrared cameras (MWIR).

The maximum thermogram in Figure 3b depicts pixel-wise the maximally emitted infrared radiation for the finished layer during the scanning of the active laser thermography with flying spot method. For this, the color scale marks lower to higher recorded values with blue to yellow. It shows a thermal signature for all of the round defects in this layer. This thermal response was caused by the interaction between the defocused process laser of the active laser thermography scanning and the loose, unmelted powder. In these areas, the maximum of the emitted infrared radiation is higher compared to the sound, solidified areas of the AM component. With this, even the smallest defects at a diameter of 400 µm are visible. Therefore, OT as in-situ monitoring and TT as in-situ NDT showed very well aligning results for defect detection. However, the thermal signature was distinctively weak for the smallest defects which might have two possible explanations: either the spatial resolution of the SWIR camera was at its limit or the actual diameter of the artificial defect in the finished layer was smaller than the nominal 400 µm. The latter might be caused by the small, omitted defect areas melting together which changes the defect appearance and reduces its diameter. However, an actual representation of the finished component with its

defect signatures (e.g., via X-ray computer tomography) would be needed. The maximum thermogram furthermore indicates on its right side the edge between component and powder bed. The defocused process laser for the scanning routine of the active laser thermography slightly struck the powder bed here. This resulted in a visible thermal response. This might be utilizable in the future to determine the actual positioning of the manufactured component in the powder bed and in the process chamber.
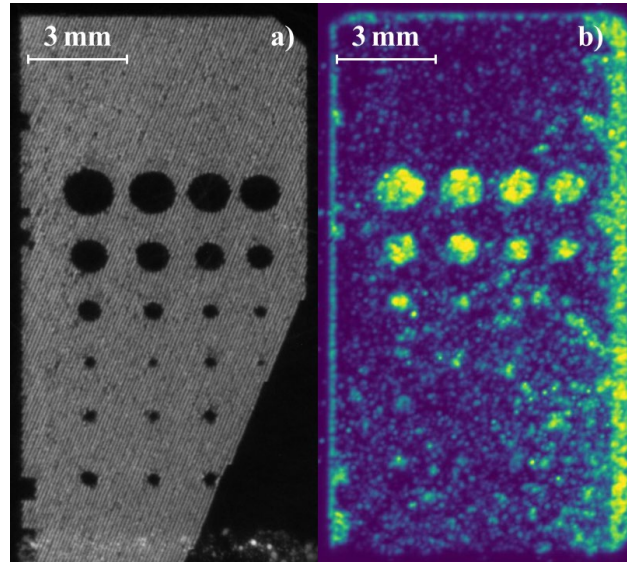

Figure 4: Optical Tomography (a) and Thermographic Testing (b) results of layer 87. Cylindrical artificial defects are at full diameters, spherical defects begin closing.

Figure 4 shows the results for OT and TT of the subsequent layer 87. On the left (a), the OT exhibits a very similar outcome to the layer before. The missing scan tracks shifted in their position due to the hatching angle changing between layers by 67 degrees. The omitted artificial defect areas are all fully visible once more. Even the top of the spherical round defects with diameters well below 400 µm are visible. Again, the high resolution of the utilized OT camera plays a part in this.

The TT results on the right (b) are similar to the layer before, but also show differences. The largest of the cylindrical defects are visible in the maximum thermogram. However, the thermal signatures of the smaller defects blend in with a decisive thermal response of the layer's surface. Due to this, the smallest defects are not clearly visible in the thermogram. Especially the top of the spherical defects with their diameters below 400 µm are not identifiable with the overlaying response pattern. Where this response stemmed from is not completely clear, but an explanation could be the rough nature of the AM surface. As the flying spot thermography is a surface NDT technique, surface inhomogeneities can negatively affect the capabilities of finding structural defects like cracks; and as severe roughness is prevalent in PBF-LB/M, the occurring thermal response as influencing factor must be under control for in-situ TT in the future. Additionally, the effect of small artificial defects melting together plays once more a role here as described above. The defect's actual extent is not clear solely from the OT as monitoring, and a ground truth would be needed.
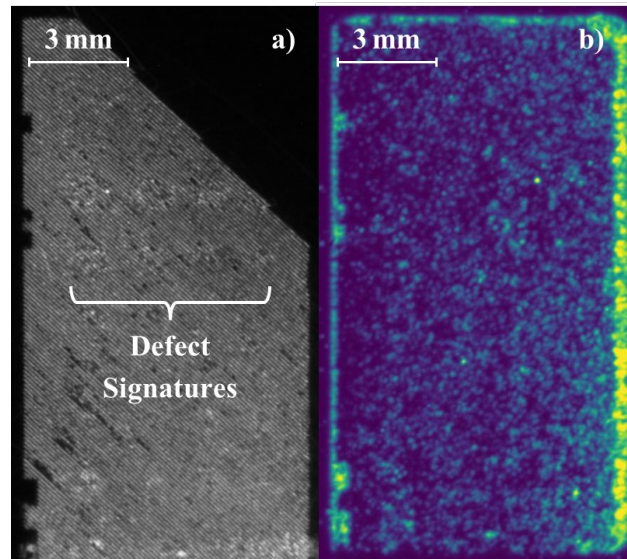
Figure 5: Optical Tomography (a) and Thermographic Testing (b) results of layer 88. First completely manufactured layer after the incorporated artificial round defects.

Layer 88 is the first complete layer without artificial defects after the defect zone. With it, the capabilities of the two applied methods (OT and TT) to find subsurface defects (in this case at 40 μm layer height) was evaluated; Figure 5 shows the results. The OT on the left (a) indicates slight signatures where the largest defects were located in the layer before. So, the emitted radiation during the build process was altered by the underlying defects and was captured integratively by the OT camera. The signatures are visible with the human eye, but they are not very distinct. This might open the possibility for future usage of artificial intelligence (AI) algorithms to detect subsurface defect signatures in OT - e.g., via convolutional neural networks (CNN). So, there is potential in high-resolution OT for quality assurance in future works.

In contrast, the maximum thermogram of layer 88 in Figure 5b does not show any signs of the subsurface defects, indicating that the chosen setting was not capable of detecting them. This is not unexpected as flying spot thermography is an active laser thermography technique that is specifically used to detect surface defects like open cracks. However, other laser excitation strategies beyond simple monodirectional scanning motions might be evaluated in the future for in-situ NDT in AM. These active laser thermography strategies are more suitable for finding subsurface defects. [9] Interestingly enough, the maximum thermogram showed a rather homogeneous thermal response across the component's surface. This contrasts the distinct thermal pattern in the subjacent layer 87 (Figure 4b). It therefore aligns more with the homogeneous thermal response of layer 86 (Figure 3b). The reason for this deviation across layers is not known at this point.
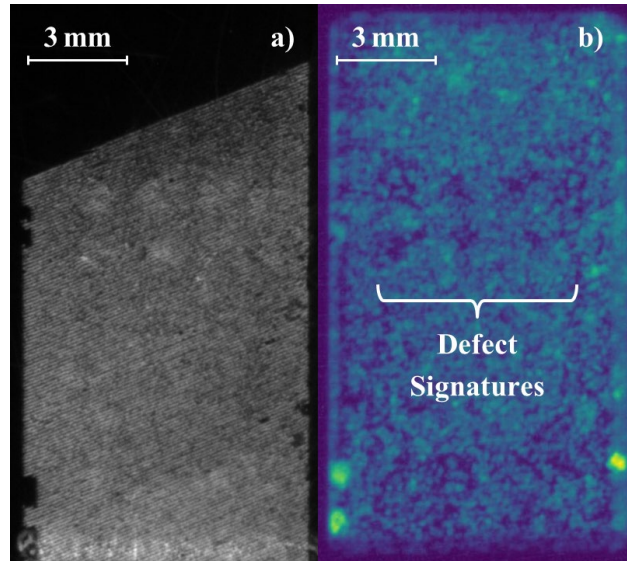
Figure 6: Optical Tomography (a) and Thermographic Testing (sum thermogram, b) results of layer 89. Second complete cover layer after the incorporated artificial round defects.

Finally, for cylindrical and spherical defects, layer 89 was analyzed - so two layers above the artificial defects at a layer height of 40 µm per layer. The results are shown in Figure 6. The OT on the left (a) still contains defect signatures of the largest artificial round defects. Obviously, they are less pronounced than before with another layer in between. However, it shows that a subsurface defect detection via monochromatic high-resolution OT might hold potential even across multiple layers.

For the TT, Figure 6b depicts the sum thermogram of layer 89. This is contrary to the maximum thermograms of Figure 3b to Figure 5b before. The exposure time t_{exp} of the SWIR camera was increased from 200 µs to 500 µs for the sum thermogram. This higher t_{exp} would result in an overexposed maximum thermogram, but for the sum thermogram, the sensitivity is beneficially increased. When considering Figure 6b, the sum thermogram shows slight defect signatures for the largest of the round defects. The results and capabilities are therefore comparable to the monitoring via OT. This indicates that a nondestructive in-situ detection of subsurface defects via active laser thermography during the AM process is possible. Background is that the sum thermogram holds information about the cooling process after the energy input of the active laser thermography. This improves the capabilities of detecting subsurface defects as defects alter the local thermal properties (e.g., cooling rate). This is then indicated in the sum thermogram. The approach holds therefore similarities to the integrative method of the OT. However, it again must be distinguished between OT as monitoring and TT as testing. The former records information about the process while the latter nondestructively assesses the actual final component. As mentioned before, the laser excitation strategy of TT can be adapted to further improve finding subsurface defects. Furthermore, comparisons of TT results and X-ray computer tomography are crucial to further evaluate the capabilities of in-situ TT. Both aspects are planned for future works.

Notch Defects

The second defect zone from layer 140 to 149 incorporated the artificial triangle and notch defects. Exemplarily, the results for layer 144 are depicted in Figure 7. The OT image on the left (a) is missing the first scan tracks because of the capture delay of the high-resolution OT camera. This

is identical to the OT images discussed beforehand for the round defects. Again, an additional delay would have prevented this and will be included for future works. Due to this, the left triangle defect structure was not recorded since its right edge was scanned separately before the rest of the layer at a different scanning angle. However, the rest of the image was fully captured and a comparison to TT is possible. The image shows that the right triangle as well as all four notches were resolved by the OT. This also includes the narrowest notch at 100 µm width. This shows that the OT as process monitoring was able to capture also fine elongated artificial defects in this configuration.
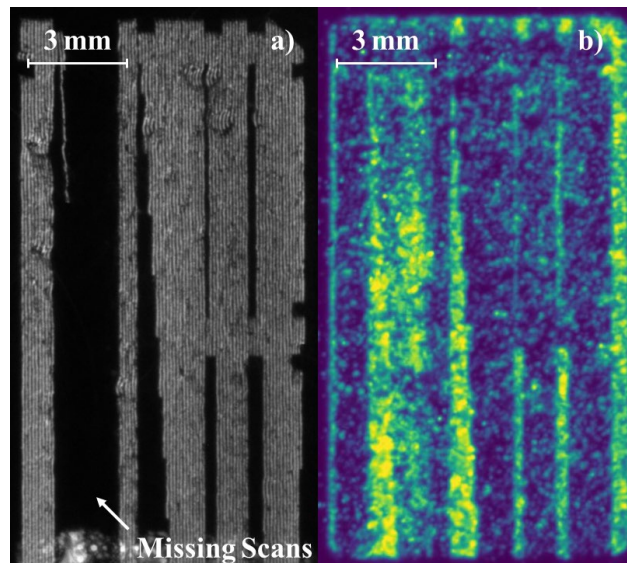

Figure 7: Optical Tomography (a) and Thermographic Testing (b) results of layer 144. Artificial triangle and notch defects are fully visible.

Figure 7b shows the maximum thermogram of the active laser thermography similarly to layers 86 to 88. The border of the powder bed and therefore the edge of the component is visible once more, most distinctly on the right edge. Both triangle defects are visible in full. Between them, an additional thermal response is located. The origin of this pattern is not identifiable at this point. All four notches were detected, even the narrowest at 100 µm. For the two notches at the lowest widths (100 µm and 200 µm), the thermal response in the maximum thermogram distinctively dropped compared to the other two, slightly wider notches. This might indicate that an effect of melting together occurred for these fine structures. Nevertheless, the TT was also able to detect all of the elongated artificial defects. In general, it showed once more that the TT as testing approach was capable of achieving comparable results in defect detection to the OT as process monitoring procedure.

The received layer information from the maximum thermograms can be stacked to obtain a quasi-3D data representation of the manufactured component. A visual representation of this is depicted in Figure 8a for the layers 140 to 149. A comparison to the 3D information from computer tomography would be feasible with this. Additionally, Figure 8b shows a photograph of the finished component. On the top, the artificial defects with triangles and notches of the second defect zone are visible. Furthermore, it shows the powder stuck in the elongated defects. It was sintered by the laser scanning of the TT and a clear increase in surface roughness is visible. Above the upper component surface, a cover layer of sintered powder was easily removed which was attached to the component. The TT was continued automatically with the PBF-LB/M process for several layers even though the investigated component was finished. This created the cover of sintered powder

and increased the surface roughness of the finished component. This further underlines the need to examine the influence of the TT's heat input on the final component quality. This examination along with the reduction of the mentioned heat input will be studied in the future.
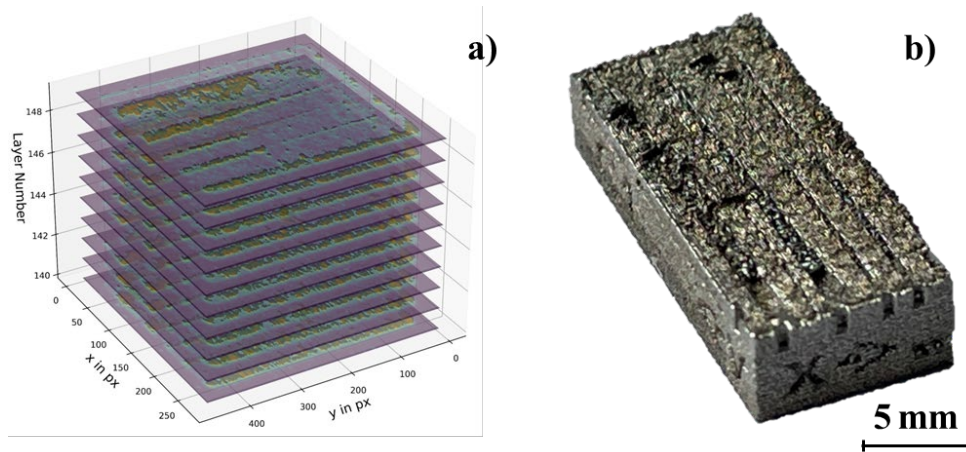

Figure 8: Layer-wise quasi-3D information from the TT for the notch defect zone at layers 140 to 149 (a) and finished component after the process (b).

Summary and Outlook

This work investigated the novel approach of including active laser thermography (TT) as nondestructive testing method into the AM process of PBF-LB/M. For this, the defocused process laser at low laser power scanned over the surface of a finished layer. The thermal response was captured via a short-wave infrared camera to detect defective regions. The capabilities of this in-situ TT approach were assessed by simultaneous comparison with optical tomography (OT). This in-situ monitoring method observes the AM process via a long-time exposure for every layer. In contrast, the TT is testing the component after each finished layer. For the investigations, a square component with artificial defects was manufactured via PBF-LB/M. The defects comprised omitted areas with round and elongated (notch) shapes at various sizes. The component was manufactured with the research machine SAMMIE using 316L stainless steel powder. The inclusion of the TT sequence after each layer was fully successful.

The results of OT and TT regarding defect display aligned very well. The two systems could successfully determine open artificial defects in AM layers. This was the case for both, round and notch defects. Even notches with a nominal width of 100 µm were detectable. For finding subsurface defects, TT with sum thermograms instead of maximum thermograms showed more promising results, but further investigation is needed.

The true extent of the defects after the process was not determinable here, and a closing of the defects by extended melting might have occurred. Due to this, a core aspect of future works on the topic will be the referencing to X-ray computer tomography (XCT) as a ground truth. The testing results from TT and the actual component information from XCT will be compared directly. Furthermore, the influence of the additional heat input on the AM component will be investigated. A reduction might be achievable by optimizing TT parameters while using cameras sensitive at longer wavelengths. The latter would decrease the minimum surface temperature at which the infrared camera captures a thermal response. Additionally, using an on-axis instead of an off-axis configuration will be beneficial for transferring the in-situ TT approach onto commercial

PBF-LB/M machines and for improved spatial resolutions. Finally, the capabilities of detecting subsurface defects might be improved by adapting the laser excitation strategy to a more sophisticated and well-suited method. Consequently, a big variety of investigations and improvements are still needed. However, the results presented within this work mark an essential step on the road from time-consuming and expensive ex-situ testing towards a nondestructive in-situ testing for AM processes.

Acknowledgement

References

[1] G. Mohr, J. Johannsen, D. Knoop, E. Gärtner, K. Hummert and C. Emmelmann, "Processing of a high-strength Al-Fe-Ni alloy using laser beam melting and its potential for in-situ graded mechanical properties," *Proceedings of the Lasers in Manufacturing Conference,* 2017.

[2] S. Oster, P. P. Breese, A. Ulbricht, G. Mohr and S. J. Altenburg, "A deep learning framework for defect prediction based on thermographic in-situ monitoring in laser powder bed fusion," *Journal of Intelligent Manufacturing,* pp. 1-20, 2023.

[3] H. Taheri, M. R. B. M. Shoaib, L. W. Koester, T. A. Bigelow, P. C. Collins and L. J. Bond, "Powder-based additive manufacturing - a review of types of defects, generation mechanisms, detection, property evaluation and metrology," *International Journal of Additive and Subtractive Materials Manufacturing,* vol. 1, no. 2, pp. 172-209, 2017.

[4] T. Becker, S. J. Altenburg, N. Scheuschner, P. P. Breese, C. Metz, K. Hilgenberg and C. Maierhofer, "In-situ monitoring of the Laser Powder Bed Fusion build process via bi-chromatic optical tomography," *Procedia CIRP,* vol. 111, pp. 340-344, 2022.

[5] J. Schlichting, M. Ziegler, C. Maierhofer and M. Kreutzbruck, "Flying Laser Spot Thermography for the Fast Detection of Surface Breaking Cracks," in *18th World Conference on Nondestructive Testing*, Durban, South Africa, 2012.

[6] F. Herzer, J. Rau, C. Seidel and J. Schilp, "Procedure for Identifying the Thermal Reaction of Defects in Solidified Layers during the PBF-LB/M Process using Active Thermography," *Procedia CIRP,* no. 118, pp. 670-675, 2023.

[7] P. P. Breese, T. Becker, S. Oster, S. J. Altenburg, C. Metz und C. Maierhofer, „Aktive Laserthermografie im L-PBF-Prozess zur in-situ Detektion von Defekten," *DGZfP-Berichtsband,* Bd. 177, 2022.

[8] B. Merz, R. G. C. Nilsson and K. Hilgenberg, "Camera-based high precision position detection for hybrid additive manufacturing with laser powder bed fusion," *The International Journal of Advanced Manufacturing Technology,* pp. 2409-2424, 2023.

[9] J. Lecompagnon, P. Hirsch, C. Rupprecht and M. Ziegler, "Influence of the number of measurements on detecting internal defects using photothermal super resolution reconstruction with random pixel patterns," *Quantitative InfraRed Thermography Journal,* 2023.